Cosmic-rays, electrons, and gamma-rays

Toru Shibata, Tomoaki Ishikawa, and Souichi Sekiguchi

Aoyama-Gakuin University, Fuchinobe 5-10-1, Sagamihara, Kanagawa, Japan 229–8558

***Abstract*. We have studied CR hadron components and electron, based on the diffusion halo model with the stochastic reacceleration, using the *same* galactic parameters. In this paper we compare our numerical results with the most recent data, focussing on the Dγs reported by FERMI-LAT. Particularly remarkable is that the FERMI-LAT data on Dγ's, though preliminary, is in good agreement with our numerical result, confirming that the EGRET GeV-excess is due to neither an astronomical origin (much harder CR spectrum in the galactic center) nor a cosmological one (dark matter annihilation), but due to an instrumental problem. We touch also recent reports on electron (positron) *anomaly* by ATIC and PAMELA in connection with the data on CRs and Dγ's.**

***Keywords*: CR electrons, propagation, reacceleration**

I. Introduction

In another paper appearing in this volume [1], hereafter referred to as Paper I, we have discussed mainly an electron component in connection with CR hadron components, and compared the numerical results with the experimental data recently reported by several groups. Aside from the prominent bump around 500 GeV, so called the ATIC-anomaly, our numerical results reproduce rather well the experimental data (see Fig. 5 in Paper I) within the uncertainties in experiments and calculations. However, looking carefully the Figure 5 in Paper I, FERMI data seem to give some deviation from our numerical curves around 500 GeV, somewhat harder than expected. This evidence might indicate some additional local sources of high energy CR electrons, or a signal of dark matter scenarios. In the present paper, however, we leave such possibilities until full results from FERMI and PAMELA, and focus our interest on the Dγ's in connection with the CR hadronic components and electron component.

II. Electron-induced γ-ray spectrum

Once we have the electron density, $N_e(\boldsymbol{r}; E_e)$, at the position $\boldsymbol{r}$ as presented in Paper I, we can obtain the electron-induced γ-ray spectrum observed at the SS, which comes from two processes, EB and IC. In this paper, we focus upon those in the energy region 1 MeV–10 GeV, as covered by COMPTEL, EGRET and FERMI, so that we discuss here the Dγ's originating from the EB and IC processes only. See [2] for Dγ's originating from the CR hadronic components, $\pi^0 \to 2\gamma$.

Here one should remember that the electron density, $N_e(\boldsymbol{r}; E_e)$, is given by equating $\bar{\epsilon}(\boldsymbol{r})$ to $\eta_0 \bar{n}(\boldsymbol{r})$, with $\eta_0 = \langle \bar{\epsilon}/\bar{n} \rangle_{\rm eff}$, where $\bar{n}(\boldsymbol{r})$ and $\bar{\epsilon}(\boldsymbol{r})$ are *smeared* gas density of ISM and energy density of ISRF respectively as discussed in Paper I. This assumption may be adequate for the *average* behavior of the electron propagation in the Galaxy, but it must be inadequate for the study of Dγ's induced by CR hadrons and electrons, particularly for the spatial distribution of Dγ's. In this paper we use separately the energy densities in two ISRFs, $\epsilon_{\rm CM}$ for IC-γ's in 2.7K-CMB medium, and $\epsilon_{\rm IR}(\boldsymbol{r})$ for IC-γ's in IR medium with the wavelength of 0.1–1000μm, in place of the average one, $\bar{\epsilon}(\boldsymbol{r})$, and the gas densities as well, $n_{\rm HI}(\boldsymbol{r})$ (HI-component), $n_{\rm HII}(\boldsymbol{r})$ (HII), and $n_{\rm H_2}(\boldsymbol{r})$ (H_2), in place of the smeared one, $\bar{n}(\boldsymbol{r})$, for EB-γ's. We don't present, however, explicit forms of these densities, but refer [3] because of limited space, which are based on the reviews by Mathis et al. [4], and Ferriere [5].

First we consider the emissivity of γ's from EB at the position $\boldsymbol{r}$, which is immediately written down as

$$q_{\rm EB}(\boldsymbol{r}; E_\gamma) = \int_{E_\gamma}^{\infty} N_e(\boldsymbol{r}; E_e) n(\boldsymbol{r}) c \sigma_{\rm EB}(E_e, E_\gamma) dE_e, \quad (1)$$

where the electron density, $N_e(\boldsymbol{r}; E_e)$, is given by Paper I (see also [3]), and the production cross-section, $\sigma_{\rm EB}(E_e, E_\gamma)$, is summarized in Table I, and see [3] for $n(\boldsymbol{r})$.

In order to perform the numerical calculation of equation (1), we need the *absolute* electron density at $\boldsymbol{r}$, $N_e(\boldsymbol{r}; E_e)$. To do so, we use the recent data on the electron intensity at the SS, $dI_e^{\odot}/dE_e$, which is related to the electron density by

$$\frac{dI_e^{\odot}}{dE_e}(E_e) = \frac{c}{4\pi} N_e(\boldsymbol{r}_{\odot}; E_e), \quad (2)$$

with $\boldsymbol{r}_{\odot} = (8.5\,\text{kpc},\ 0)$. In practice, we normalize the electron density at $E_s = 10\,\text{GeV}$ with use of the data now available (see Fig. 5 in Paper I), where the solar modulation effect is negligible,

$$cN_s^{\odot} \equiv cN_e(\boldsymbol{r}_{\odot}; E_s) = 0.219\ \text{m}^{-2}\text{s}^{-1}\text{GeV}^{-1}. \quad (3)$$

The uncertainty in the normalized intensity is as large as 10% around $E_e \approx E_s$, much less than that in the higher energy region, $\gtrsim 100\,\text{GeV}$. On the other hand, for the hadron-induced γ's ($\pi^0 \to 2\gamma$), the normalization energy is set to $100\,\text{GeV nucleon}^{-1}$ [2].

Now taking care of the terms related to $\boldsymbol{r}$, we have the following result

$$\frac{q_{\rm EB}(\boldsymbol{r}; E_\gamma)}{n(\boldsymbol{r}) w_{\rm EB}^{(0)} N_s^{\odot}} = \text{e}^{-u_{\odot}(\boldsymbol{r})} \int_0^1 \phi_{\rm EB}(E_\gamma, x) \frac{F_r(E_x)}{F_{\odot}(E_s)} \frac{dx}{x^2}, \quad (4)$$

TABLE I: Summary of the production cross-sections of γ-rays in the EB and the IC processes, where E_e is the incident energy of electron, and E_γ is the energy of the produced γ's, with $x = E_\gamma/E_e$ in both processes, and E the energy of the target photon before electron scattering. For the EB process, we present the cross-section in the case of only one-electron atoms, see Gould [12] for two-electron atoms.

bremsstrahlung (EB)	inverse compton (IC)
$\sigma_{\rm EB}(E_e,E_\gamma)dE_\gamma = \sigma_{\rm EB}^{(0)}\phi_{\rm EB}(E_\gamma,x)\dfrac{dx}{x}$	$\sigma_{\rm IC}(E_e,E_\gamma;E)dE_\gamma = \sigma_{\rm IC}^{(0)}\phi_{\rm IC}(q,x)\dfrac{dx}{X}$
$\sigma_{\rm EB}^{(0)} = 4\alpha_f Z(Z+1)[e^2/m_ec^2]^2;\quad \alpha_f = 1/137$	$\sigma_{\rm IC}^{(0)} = 3\sigma_{\rm Th} = 8\pi[e^2/(m_ec^2)]^2$
$\phi_{\rm EB}(E_\gamma,x) = [1+(1-x)^2]\phi_1(\delta,x) - \dfrac{2}{3}(1-x)\phi_2(\delta,x)$	$\phi_{\rm IC}(q,x) = 2q\ln q + (1-q)\left(1+2q+\dfrac{1}{2}\dfrac{x^2}{1-x}\right)$
$\phi_1(\delta,x) = 1 + \displaystyle\int_\delta^1 dy\phi_0(y)(y-\delta)^2;\quad \delta\equiv\delta(E_\gamma,x)$	$q \equiv q(x,X) = \dfrac{x}{1-x}\dfrac{1}{X}$
$\phi_2(\delta,x) = \dfrac{5}{6} + \displaystyle\int_\delta^1 dy\phi_0(y)\left\{y^2 + 3\delta^2\left(1+\ln\dfrac{\delta^2}{y^2}\right) - \dfrac{4\delta^3}{y}\right\}$	$X \equiv X(EE_e) = \dfrac{4EE_e}{(m_ec^2)^2}$
$\phi_0(y) = 1 - \dfrac{1}{[1+y^2/(2\alpha_f Z)^2]^2};\quad \delta(E_\gamma,x) = \dfrac{x^2}{1-x}\dfrac{m_ec^2}{2E_\gamma}$	

$$u_\odot(\boldsymbol{r}) \simeq \left(\frac{z_n}{z_Q}-1\right)\frac{r-r_\odot}{r_n} + \frac{|z|}{z_D}, \tag{5}$$

with $x = E_\gamma/E_e$, $E_x = E_\gamma/x$, where $w_{\rm EB}^{(0)} = c\sigma_{\rm EB}^{(0)} = 1.39\times10^{-16}\,{\rm GeV\,s^{-1}}$ for the hydrogen gas ($Z=1$), and see the left-hand side of Table I for $\sigma_{\rm EB}^{(0)}$ and $\phi_{\rm EB}(E_\gamma,x)$. See also Paper I for $F_r(E_e)$ and the scale height parameters, z_n, z_D, ...

The emissivity of γ's coming from the IC process is somewhat complicated, as there are several kinds of target photons with different energy density as well as with different scale heights in the spatial gradient. Here we present only the results corresponding to eq. (4)

$$\frac{q_{\rm CM}(\boldsymbol{r};E_\gamma)}{\epsilon_{\rm CM}w_{\rm Th}N_s^\odot} = {\rm e}^{-u_\odot(\boldsymbol{r})}\int_0^1 \Phi_{\rm CM}(E_\gamma,x)\frac{F_r(E_x)}{F_\odot(E_s)}\frac{dx}{x^2}, \tag{6a}$$

$$\frac{q_{\rm IR}(\boldsymbol{r};E_\gamma)}{\epsilon_{\rm IR}(\boldsymbol{r})w_{\rm Th}N_s^\odot} = {\rm e}^{-u_\odot(\boldsymbol{r})}\int_0^1 \Phi_{\rm IR}(E_\gamma,x)\frac{F_r(E_x)}{F_\odot(E_s)}\frac{dx}{x^2}, \tag{6b}$$

with $w_{\rm Th} = 1.018\times10^{-16}\,{\rm GeV\,s^{-1}}$, $\epsilon_{\rm CM} = 0.261\,{\rm eV\,cm^{-3}}$, and $\epsilon_{\rm IR}(\boldsymbol{r})$ is the energy density of IR at $\boldsymbol{r}$. The first one (6a) corresponds to electron-CMB, and the second one (6b) to electron-IR, see [3] for complete forms.

Once we have the emissivity of γ's induced by the interaction between the electron and radiation fields, ISM and ISRF, we can obtain immediately the intensity of γ's observed at the SS, $\boldsymbol{r}_\odot(r_\odot,0)$, coming from the direction $\boldsymbol{\theta}(l,b)$:

$$\frac{d^3I_\gamma^\odot(E_\gamma;\boldsymbol{\theta})}{dE_\gamma dl d(\sin b)} = \frac{1}{4\pi}\int_0^\infty q_\gamma(\boldsymbol{r};E_\gamma)ds, \tag{7}$$

with

$$q_\gamma(\boldsymbol{r};E_\gamma) = q_{\rm EB}(\boldsymbol{r};E_\gamma) + q_{\rm CM}(\boldsymbol{r};E_\gamma) + q_{\rm IR}(\boldsymbol{r};E_\gamma), \tag{8}$$

where $q_{\rm EB}(\boldsymbol{r};E_\gamma)$, $q_{\rm CM}(\boldsymbol{r};E_\gamma)$, and $q_{\rm IR}(\boldsymbol{r};E_\gamma)$ are presented in eqs. (4-6), and the integration with respect to s is performed along the arrival direction of γ's, $\boldsymbol{\theta}(l,b)$, at the SS, and $\boldsymbol{r}(r,z)$ is bound to $(s;\,l,b)$ as follows,

$$r(s;\,l,b) = \sqrt{r_\odot^2 + s^2\cos^2 b - 2r_\odot s\cos b\,\cos l}, \tag{9a}$$

$$z(s;\,b) = s\sin b. \tag{9b}$$

Now we can obtain the energy spectrum within a solid angle, $\Delta\Omega \equiv \Delta l\Delta\sin b$ with $\Delta l = l_2 - l_1$ and $\Delta\sin b = \sin b_2 - \sin b_1$, and two lateral distributions, the longitudinal and latitudinal ones, for the energy interval, $\Delta E_\gamma = E_2 - E_1$, are given by numerical results of which are presented in the next section together with the experimental data.

III. RESULTS

There are three sources of Dγ's, (1) hadron-induced one ($\pi^0 \to 2\gamma$), (2) electron-induced one (EB and IC), and (3) the extragalactic (EG) one. The first has already been presented in detail in [2], though neglecting the EG background, and the second one is discussed in previous section. The EG Dγ flux is obtained from the latitudinal distribution of Dγ', so that we start from the spatial distributions of Dγ's in order to obtain the flux of EG component.

In Figure 1, we present an example of EGRET data (*histogram*) [6] on the latitudinal distribution averaged over full longitude ranges, 0°–360° with the energy interval of 300–500 MeV, where we give the contributions of Dγ's separately from π^0, EB, IC, EG, and total flux,

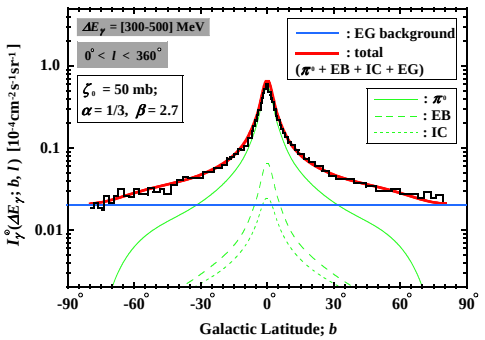

Fig. 1: Example of the estimation of the extragalactic (EG) background using the latitudinal Dγ's data from EGRET with the energy interval of 300-500 MeV over the whole radial direction.

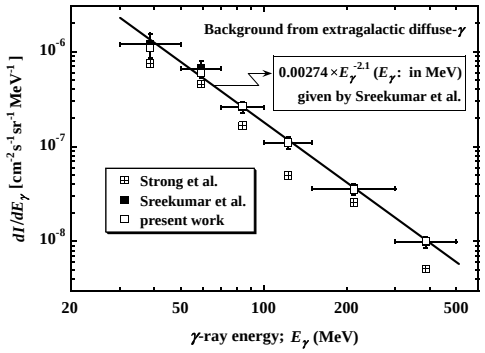

Fig. 2: The extragalactic Dγ emission spectrum.

π^0+EB+IC+EG, assuming $\beta = 2.7$ with $(\alpha, \zeta_0, \eta_0) = (\frac{1}{3}$, 50 mbarn, 5 eV) (see Paper I for the definition of these parameters). It is remarkable that the numerical curve is in good agreement with the data within the ranges of approximately $\pm 5^\circ$ not only in the shape, but also in the absolute value. One can see clearly a lengthy tail coming from the EG background at high latitudes. In the present paper, we draw a horizontal line (*solid blue*) by eye so that the histogram at high latitudes is well reproduced.

In Figure 2, we present the intensity of EG-Dγ emission thus obtained (*open squares*), where also plotted are the results of Sreekumar et al. [7] and Strong et al. [8], together with a straight line with the index of -2.1 given by the former authors. We find that our results

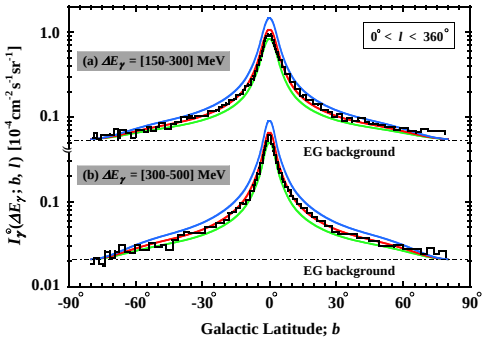

Fig. 3: Latitudinal distribution of Dγ's for energy intervals, (a) [150-300] MeV and (b) [300-500] MeV.

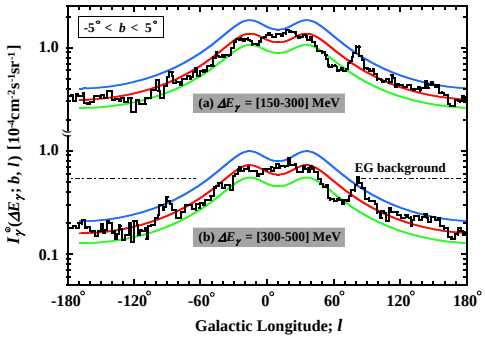

Fig. 4: Longitudinal distribution of Dγ's for energy intervals, (a) [150-300] MeV and (b) [300-500] MeV.

are almost the same as those of Sreekumar et al., while those by Strong et al. give a significantly lower intensity.

We give the latitudinal distributions for two energy ranges in Figure 3, (a) ΔE_γ = 150–300MeV, (b) 300–500MeV, together with our numerical results taking the EG contribution into account as mentioned above, where we plot three curves for each figure with $\beta = 2.6$ (*green*), 2.7 (*red*), and 2.8 (*blue*). One finds the agreement between the data and the curves is quite satisfactory.

Corresponding to the latitudinal distributions as shown in Figure 3, we demonstrate the longitudinal distributions for two energy ranges in Figure 4. Again we find the numerical results are in good agreement with the data both in shape and absolute value.

Now, we compare the energy spectrum of EGRET-Dγ emission with our numerical results for several angles of the field of view, $(\Delta l, \Delta b)$. In Figure 5 we present the energy spectrum averaged over the field of view with $300^\circ < l < 60^\circ$ and $|b| < 10^\circ$, where four components are shown, π^0, EB+IC, EG, and total ($\equiv \pi^0 + \mathrm{EB} + \mathrm{IC} + \mathrm{EG}$), each for three values of β, 2.6, 2.7 and 2.8, based on the reacceleration model. The straight line of EG is given by Sreekumar et al. [7] appearing in Figure 2. One finds the curve with $\beta = 2.7$ is in good agreement with the data in the energy region below 1 GeV, while the data deviates significantly from our curves above 1 GeV, which will be discussed below.

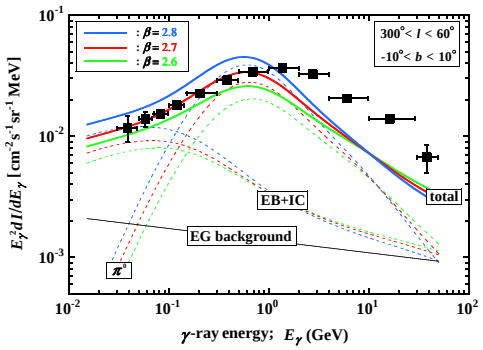

Fig. 5: Differential energy spectra of Dγ's, with $300^\circ < l < 60^\circ$ and $|b| \leq 10^\circ$.

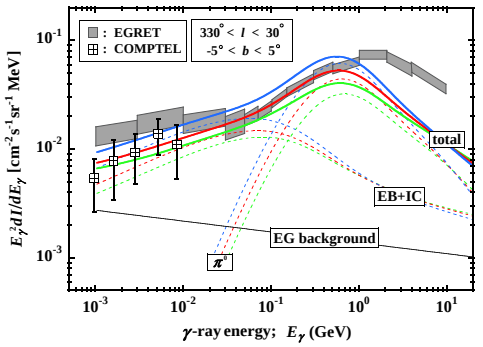

Fig. 6: Same as Figure 5, but with different field of view, $330^\circ < l < 30^\circ$ and $|b| \leq 5^\circ$, covering wide energy intervals, from 1 MeV to 10 GeV.

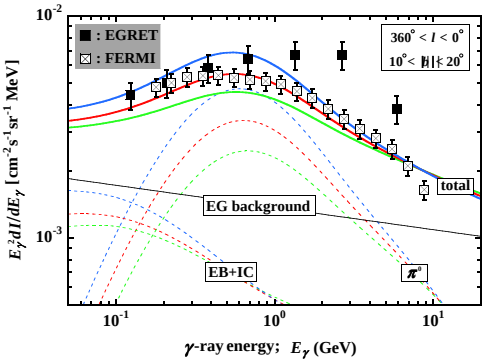

Fig. 7: Same as Figure 5, with preliminary FERMI data, where the field of view is $360^\circ < l < 0^\circ$ and $10^\circ \leq |b| \leq 20^\circ$.

Next we present the energy spectrum in the wide energy ranges, 1 MeV to 10 GeV, in Figure 6, averaged over the field of view with $330^\circ < l < 30^\circ$ and $|b| < 5^\circ$, where COMPTEL data [9] are also plotted, and we draw curves separately with the same four components as in Figure 5. Again we find a good fit with the data in the energy region less than 1 GeV, while our model seems to fit the COMPTEL data well in the low energy region, $\lesssim$ 10 MeV.

Finally, we compare our numerical results with the most recent, albeit preliminary, data from FERMI [10], averaged over the field of view with $360^\circ < l < 0^\circ$ and $10^\circ < |b| < 20^\circ$, where EGRET data are also plotted. First one finds that the FERMI data do not confirm the EGRET GeV-excess. Second it is remarkable that the numerical curves with $\beta = 2.7$–2.8 reproduce the FERMI data quite well. So it is desirable that the energy ranges are extended to both lower regions, $\lesssim$ 100 MeV, and higher regions, $\gtrsim$ 10 GeV. In particular, it is important to extend coverage to more than 100 GeV where ground-based telescopes such as H.E.S.S. and MAGIC are now providing data.

IV. Discussion

We have studied the diffusion-halo model with stochastic reacceleration, comparing with the most recent data on hadronic, electronic and Dγ components, in Paper I and in the present paper. We have two particular interests: to find an unified model for the CR acceleration and propagation from the view point of astrophysics, and to search for a signal of novel sources such as PBH and/or DM from the view points of particle physics and cosmology. Both are of course closely connected with each other in the sense that the knowledge of the former is decisive in confirming the latter. Particularly nowadays, several groups have reported a possibility of annihilation of DM particles, giving a significant excess (enhancement) in electron (positron) flux (see Paper I and references therin), which might bring a new window for particle physics and astrophysics.

While FERMI-LAT and HESS report most recently no prominent bump in electron spectrum around 600 GeV by ATIC and PPB-BETS (see Paper I), we can not still exclude additional components such as dark matter particles and/or local sources. Anyway we await full results of FERMI and PAMELA, and also further analysis in HESS and MAGIC.

Aside from the electron-anomaly problems, we find that the diffusion-halo model with the reacceleration with the parameter set, (β, α, ζ_0) = (2.7–2.8, $\frac{1}{3}$, 50 mbarn), is in harmony with the CR hadron data presently available. The most recent data on the B/C ratio by CREAM, and $\bar{p}/p$ ratio by PAMELA (Figs. 3 and 4 in Pper I) also support the present model.

However, it is worth mentioning here that our interpretation for the energy dependence of the B/C ratio is somewhat different from that by CREAM team. They comment that the index α favors 0.5–0.6 instead of $\frac{1}{3}$, resulting in a rapid decrease with energy for the interstellar propagation pathlength.

In contrast to their interpretation, we would like to point out that the value of 0.5–0.6 is not *fundamental*, but is rather due to the reacceleration effect, namely it is boosted upward around the GeV region by the energy gain, resulting in *accidentally* the soft slope with 0.5–0.6 in the energy region of 1–100 GeV. The intrinsic one must be $\frac{1}{3}$ (Kolmogorov-type spectrum in hydromagnetic turbulence), leading to a natural drop in path length distribution in the low energy region $\lesssim$ 1 GeV without introducing an artificial ad hoc break there, which was originally proposed by Simon et al. [11].

We applied the diffusion-halo model for the electron component (Fig. 5 in Paper I), and Dγ's (Fig. 7), and find that the numerical results using the same parameters as those assumed in hadronic components reproduce well them, while FERMI electron data seem to give somewhat hard spectrum as compared to the curves. About these deviations, we shall discuss separately in the future.

Through the studies of Dγ's, we find that the contributions from π^0, EB, IC, and EG, depend significantly on the energy as well as on the direction of field of view, for instance EG γ's become dominant even below 10 GeV (Fig. 7) for the field of view with $0^\circ < l < 360^\circ$ and $10^\circ < |b| < 20^\circ$. It is critically important to see which component contributes to the Dγ's, particularly for the TeV-γ astronomy with ground-based telescopes, which will be reported elsewhere.

References

[1] Shibata, T., et al. 2009, this volume in the conference paper
[2] Shibata, T., et al. 2007, Astrop. Phys. 27, 411
[3] Shibata, T., submitted to ApJ.
[4] Mathis, J. S., et al. 1983, A&A, 128, 212
[5] Ferriere, K. M. 2001, Rev. Mod. Phys., 73, 1031
[6] Hunter, S. D. et al., 1997, ApJ, 481, 205
[7] Sreekumar, P. et al., 1998, ApJ, 494, 523
[8] Strong, A. W. et al., 2000, ApJ, 537, 763
[9] Strong, A. W. et al., 1999, Astrophys. Lett. Commun., 537, 763
[10] Porter, T., et al. (FERMI-LAT), Symp. on First results from Fermi Gamma-Ray Space Telescope, held at Tokyo Inst. of Tech. on March 7, 2009
[11] Simon, M. et al., 1986, ApJ, 300, 32
[12] Gould, R. J. 1969, Phys. Rev., 185, 72